Title

Human eukaryotic initiation factor 4G directly binds the 40S ribosomal subunit to promote efficient translation

Journal

Journal of Biological Chemistry, 300(5)

ISSN

0021-9258

Authors

Villa, Nancy

Fraser, Christopher S

Publication Date

2024-05-01

DOI

10.1016/j.jbc.2024.107242

Peer reviewed

Human eukaryotic initiation factor 4G directly binds the 40S ribosomal subunit to promote efficient translation

Received for publication, September 30, 2023, and in revised form, March 15, 2024 Published, Papers in Press, April 1, 2024,
https://doi.org/10.1016/j.jbc.2024.107242

Nancy Villa and Christopher S. Fraser*

From the Department of Molecular and Cellular Biology, College of Biological Sciences, University of California, Davis, California, USA

Reviewed by members of the JBC Editorial Board. Edited by Ronald Wek

Messenger RNA (mRNA) recruitment to the 40S ribosomal subunit is mediated by eukaryotic initiation factor 4F (eIF4F). This complex includes three subunits: eIF4E (m^7G cap-binding protein), eIF4A (DEAD-box helicase), and eIF4G. Mammalian eIF4G is a scaffold that coordinates the activities of eIF4E and eIF4A and provides a bridge to connect the mRNA and 40S ribosomal subunit through its interaction with eIF3. While the roles of many eIF4G binding domains are relatively clear, the precise function of RNA binding by eIF4G remains to be elucidated. In this work, we used an eIF4G-dependent translation assay to reveal that the RNA binding domain (eIF4G-RBD; amino acids 682–720) stimulates translation. This stimulating activity is observed when eIF4G is independently tethered to an internal region of the mRNA, suggesting that the eIF4G-RBD promotes translation by a mechanism that is independent of the m^7G cap and mRNA tethering. Using a kinetic helicase assay, we show that the eIF4G-RBD has a minimal effect on eIF4A helicase activity, demonstrating that the eIF4G-RBD is not required to coordinate eIF4F-dependent duplex unwinding. Unexpectedly, native gel electrophoresis and fluorescence polarization assays reveal a previously unidentified direct interaction between eIF4G and the 40S subunit. Using binding assays, our data show that this 40S subunit interaction is separate from the previously characterized interaction between eIF4G and eIF3. Thus, our work reveals how eIF4F can bind to the 40S subunit using eIF3-dependent and eIF3-independent binding domains to promote translation initiation.

Messenger RNAs (mRNA) are selected for translation through recognition of key features including the 5′ 7-methylguanosine (m^7G) cap and the 3′ poly(A) tail. Selection is mediated by the cap-binding complex, eukaryotic initiation factor (eIF) 4F, and is a highly regulated step of translation initiation (1–5). eIF4F is composed of the m^7G cap binding protein named eIF4E, a DEAD-box helicase named eIF4A, and a scaffold protein named eIF4G (reviewed in (6)). The eIF4G protein binds and coordinates the activities of eIF4E, eIF4A, and poly(A) binding protein (PABP). In mammals, mRNA recruitment to the 40S subunit is thought to be promoted by the direct interaction between eIF4G and the multi-subunit eIF3, which makes critical contact with the 40S subunit. Consistent with this model, a truncated eIF4G that does not include the eIF3 binding domain cannot initiate translation in an eIF4G-dependent assay (7). A number of contacts between eIF4G, eIF3, and the 40S subunit have been observed in a recent cryo-EM model of the 48S complex, but it should be noted that the region surrounding the interaction of the eIF4F complex with eIF3 is of modest resolution (8). Following recruitment, the 40S subunit will scan along the mRNA in a 5′ to 3′ direction until it recognizes the start codon (usually AUG). Following this, initiation factors are released from the 40S, and the 80S ribosome is formed to begin the elongation phase of translation.

As a scaffolding protein, human eIF4G1 consists of a single 175 kDa polypeptide that contains several binding domains to promote mRNA recognition and translation (9, 10). Conceptually, eIF4G can be divided into functional thirds (Fig. 1*A*). The N-terminal third of the protein is delineated by cleavage sites for foot-and-mouth disease virus (FMDV) L protease (L^{pro}) and poliovirus 2A protease ($2A^{pro}$). This region contains binding sites for eIF4E (9, 11) and PABP (12, 13). The central third of eIF4G extends approximately from amino acids 682 to 1104 ($eIF4G_{682\text{-}1104}$). It contains RNA (14–16), eIF4A (17, 18), and eIF3 (9, 18) binding regions and has been identified as the "functional core" of the protein, as defined by its ability to promote mRNA recruitment to the 40S subunit (19, 20). The C-terminal third of eIF4G binds the eIF4E kinase MAPK-activated protein kinase 1 (MNK1) (14) and has a second binding site for eIF4A (9, 15–17).

The roles of the eIF4A and eIF3 binding regions in the eIF4G core have become established, but the precise role, and even the requirement for, RNA binding to this core domain remains unclear. Crosslinking between eIF4E and the mRNA cap shows that eIF4G•eIF4E binding increases m^7G cap association of eIF4E when recombinant eIF4G constructs added to the reaction contained the RNA binding region (21, 22). Replacing the native RNA binding domain with that of the RNA recognition motif 1 (RRM1) of the La autoantigen showed that this effect was not sequence-specific. Thus, the eIF4G interaction with mRNA may simply serve to tether its associated eIF4E and increase its local concentration near the cap, thereby promoting m^7G cap binding and translation (22).

* For correspondence: Christopher S. Fraser, csfraser@ucdavis.edu.

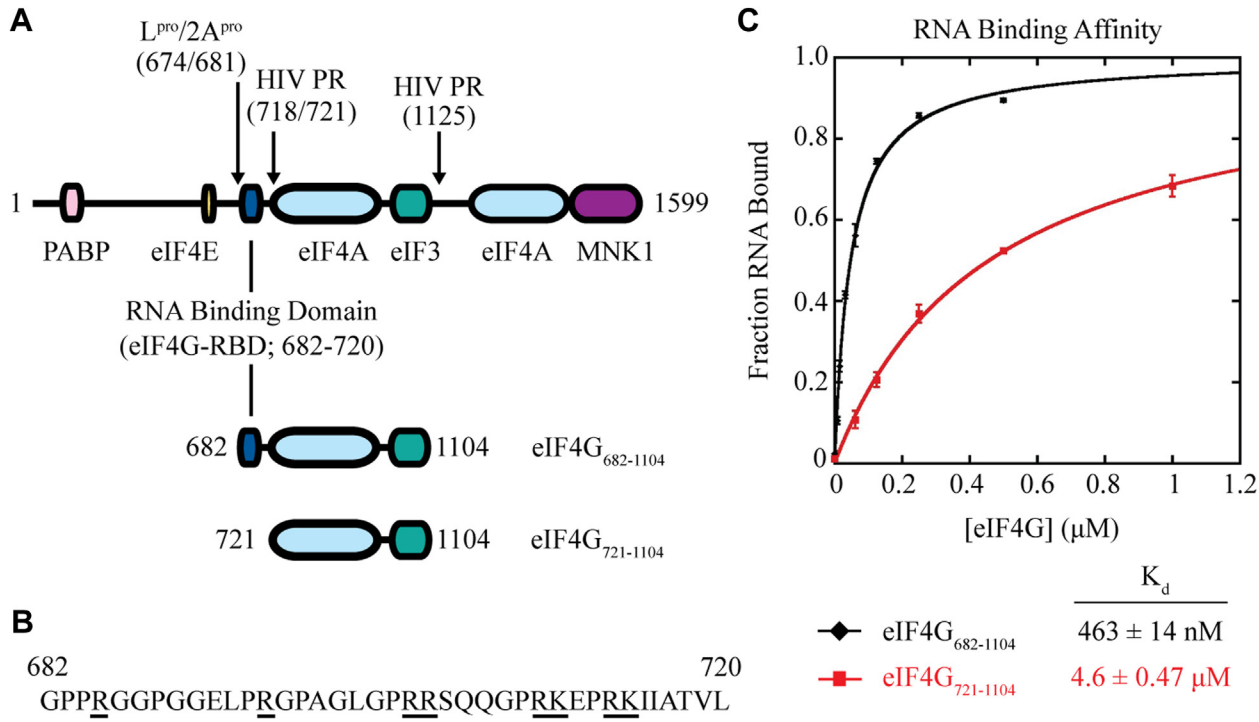

Figure 1. The eIF4G-RBD is required for high-affinity RNA binding. *A*, domain map of full-length human eIF4GI and constructs used in this study. FMDV L protease (L^{pro}), Poliovirus 2A protease ($2A^{pro}$), and HIV-1 protease (HIV PR) cleavage sites are noted. The eIF4G-RBD (amino acids 682–720) is included in $eIF4G_{682-1104}$ and truncated in $eIF4G_{721-1104}$ to study the function of this domain. Each construct is tagged and mutated as noted in subsequent figures and legends. *B*, amino acid sequence of the eIF4G-RBD, with positively charged amino acids underlined. *C*, fluorescence polarization assays are used to determine the equilibrium dissociation constant (K_d) of the eIF4G•RNA interaction using a 42 nucleotide 3′-end fluorescein-labeled RNA. The fraction of RNA bound by $eIF4G_{682-1104}$ (*black*), or $eIF4G_{721-1104}$ (*red*), is the average of at least three trials and error bars indicate the SEM.

Nevertheless, one limitation of these experiments is that a crosslinking assay was used to monitor the formation of eIF4F on m^7G-capped mRNA. Thus, while these studies begin to explain the role of the eIF4G RNA binding domain as a tether to the mRNA, quantitative binding and translation assays are needed to fully characterize the function of this domain.

In *S. cerevisiae*, eIF4G contains 3 RNA binding domains, RNA1, -2, and -3, where RNA2 is in the same relative position (between the eIF4E and eIF4A binding sites) as the human eIF4G RNA binding domain. The eIF4G•eIF4E interaction was shown to not be essential in yeast, as eIF4G mutants impaired in this function were still viable. However, RNA2 deletion, eIF4E-binding double mutants were lethal despite retaining the ability to form eIF4G•PABP•mRNA complexes. These results suggest that RNA2 has an essential, non-redundant function beyond binding mRNA that is independent of the eIF4G•eIF4E interaction (23). While this RNA binding domain bears little sequence similarity between species, its comparable position within yeast and human eIF4G proteins suggests that human eIF4G may bear similar, though yet undefined important functions. Throughout this manuscript, we will refer to this RNA binding domain in mammalian eIF4G1 (amino acids 682–720) as the eIF4G-RBD.

In mammalian cap-dependent translation, eIF4G bridges the mRNA and 40S subunit through its interactions with both eIF4E via its N-terminal binding domain and eIF3 via its binding domain in the eIF4G core. To promote viral protein synthesis during infection, both $2A^{pro}$ and L^{pro} cleave eIF4G to separate the N-terminal third from the middle and C-terminal domains, thereby reducing competition for the translation machinery from capped, endogenous mRNAs (24–26). Human immunodeficiency virus proteases (HIV-1 and HIV-2 PR) also inhibit cellular translation by targeting eIF4G, most notably cleaving just before amino acids 718/721, which is between the eIF4G-RBD and the eIF4A binding region (27–29). This results in a core domain containing only the eIF4A and eIF3 binding sites or a fragment that extends to the C-terminal end of the protein if the secondary site at amino acid 1125 is not cleaved (15, 28). Protease cleavage of eIF4G in rabbit reticulocyte lysate (RRL) followed by centrifugation to pellet ribosomes and associated factors showed that L^{pro}-cleaved eIF4G remains bound to ribosomes and eIF3 in the pellet, whereas eIF4G cleaved with HIV-2 PR, which removes the eIF4G-RBD, is released into the supernatant (15). These results indicate a possible role for the eIF4G-RBD of mammalian eIF4G in 48S complex formation, although it is also possible the effect was indirectly due to HIV-2 PR targeting other components of the RRL, such as eIF3 subunit d (eIF3d) which is known to bind eIF4G (7, 15, 30).

In this work, we investigate the specific role of the eIF4G-RBD. Using an eIF4G-dependent RRL system, we compare translation directed by two different eIF4G constructs: $eIF4G_{682-1104}$, the eIF4G core that contains the eIF4G-RBD, and $eIF4G_{721-1104}$, which is N-terminally truncated and does not contain the eIF4G-RBD (Fig. 1, *A* and *B*). We find that while $eIF4G_{721-1104}$ is capable of initiating translation, the

eIF4G-RBD stimulates translation by about 1.5–2-fold. Unexpectedly, we identify a direct interaction between eIF4G and the 40S subunit. This interaction is dependent on the eIF4G-RBD, but independent of its role in promoting eIF4A-dependent helicase activity and tethering eIF4F to the mRNA. Finally, we show that the eIF4G-RBD provides a direct binding site to the 40S subunit that is separate from the interaction between eIF4G and the eIF3 complex.

Results

The eIF4G-RBD is required for high-affinity RNA binding to eIF4G$_{682-1104}$

Published studies have helped to locate and attribute general non-specific RNA binding properties to the human eIF4G-RBD (amino acids 682–720), showing it promotes binding to both the internal ribosomal entry site of encephalomyocarditis virus (EMCV) and β-globin RNA, without an apparent common preference for specific RNA structures or sequence (Fig. 1, *A* and *B*) (14, 16, 22, 31). The eIF4G-RBD has been proposed to help tether eIF4F to a cellular mRNA or a subset of factors to a viral transcript for ribosome recruitment. To determine the precise effect of the eIF4G-RBD on RNA binding by eIF4G, we first used a steady-state fluorescence polarization assay (32). We compared the equilibrium dissociation constant (K_d) of a 42 nucleotide 3′-end fluorescein-labeled RNA (CAA-42-FL) and eIF4G in the presence (eIF4G$_{682-1104}$) or absence (eIF4G$_{721-1104}$) of the eIF4G-RBD (Fig. 1*A*). The change in fluorescence anisotropy that was specific to eIF4G$_{682-1104}$ or eIF4G$_{721-1104}$ was measured, as described in *Experimental Procedures*. A strong anisotropy increase upon titration of either eIF4G construct was observed, indicating productive binding to form a complex with CAA-42-FL (Fig. 1*C*). Converting anisotropy values into the fraction of CAA-42-FL bound at each eIF4G concentration yields a K_d of 463 ± 14 nM for eIF4G$_{682-1104}$ and 4.60 ± 0.47 μM for eIF4G$_{721-1104}$ (Fig. 1*C*; see Table 1 for K_d values). Thus, eIF4G$_{682-1104}$ binds RNA with a ∼10-fold greater affinity than eIF4G$_{721-1104}$. Together, these data and previously published work show that the eIF4G-RBD provides a non-specific RNA binding affinity for the core eIF4G domain (14, 16, 22, 31).

The eIF4G-RBD promotes translation initiation independent of mRNA tethering

We next used an eIF4G-dependent translation assay in nuclease-treated RRL to determine the role of the eIF4G-RBD in translation. This assay was adapted from work by the Hentze lab, where an eIF4G "ribosome recruitment core" was identified *in vivo* to include amino acids 682 to 1131 that contains the eIF4G-RBD, the central eIF4A binding domain, and the eIF3 binding domain (19). Our lab showed that a similar eIF4G truncation (eIF4G$_{682-1104}$) can efficiently recruit ribosomes to a transcript for translation using an RRL system (7). For this assay, a renilla luciferase reporter RNA with an engineered boxB hairpin in the 5′ UTR specifically recruits a 22 amino acid sequence of the bacteriophage λ transcription anti-terminator protein N (λN). Using the boxB hairpin, λ-eIF4G is directed to the reporter RNA independent of eIF4E, and ribosomes are recruited solely through interaction with λ-eIF4G. Luciferase translation is initiated by the addition of recombinant purified λ-eIF4G to the lysate, and 5′-end dependent initiation is prohibited by the inhibitory hairpin placed at the 5′-end of the uncapped RNA (Fig. 2*A*). The boxB•λN interaction has a reported picomolar affinity, which ensures any λ-eIF4G proteins added to the RRL will be efficiently tethered at low concentrations to the RNA template to recruit ribosomes (7, 19, 33, 34). As described in *Experimental Procedures*, we optimized our translation buffer conditions so that translation of the boxB reporter construct is λ-eIF4G-dependent (Fig. S1 and Table S1), which is similar to the boxB buffer conditions we used previously (35). We further confirmed the activity of our RRL system by comparing the translation activity of the boxB construct to un-capped and m^{7}G-capped globin UTR reporters under "Kozak" and "boxB" translation buffer conditions (Fig. S1 and Table S1) (36).

To test the independent role of the eIF4G-RBD in regulating translation, we compared the translation activity of λ-eIF4G$_{682-1104}$ versus the eIF4G-RBD truncation λ-eIF4G$_{721-1104}$. We measured luciferase translation using increasing concentrations of λ-eIF4G to calculate the apparent equilibrium dissociation constant ($K_{d,app}$) as well as the maximum relative translation activity (T_{Max}) of each complex. Calculating $K_{d,app}$ is needed to determine whether any differences in observed translation are due to differences in affinity or activity

Table 1
Summary of equilibrium binding parameters

Figures	Labeled molecule	Complex bound	K_d[a] (nM)	r_{free}[b]	r_{bound}[c]	Δr_{max}[d]
Figure 1	42mer-3′Fl	eIF4G$_{682-1104}$	463 ± 14	0.097 ± 0.003	0.240 ± 0.001	0.143 ± 0.003
		eIF4G$_{711-1104}$	4605 ± 467	0.100 ± 0.001	0.232 ± 0.006	0.132 ± 0.005
Figure 5	eIF4G$_{682-1104}$-Fl (E711C)	eIF4A + 40S	129 ± 9	0.133 ± 0.002	0.176 ± 0.001	0.043 ± 0.004
		eIF4A + eIF3[e] + 40S	76 ± 4	0.152 ± 0.002	0.182 ± 0.002	0.030 ± 0.002
	eIF4G$_{711-1104}$-Fl (E711C)	eIF4A + 40S	563 ± 72	0.129 ± 0.001	0.156 ± 0.002	0.027 ± 0.001
		eIF4A + eIF3[e] + 40S	248 ± 64	0.144 ± 0.001	0.155 ± 0.001	0.011 ± 0.002
Figure 6	eIF4G$_{721-1104}$-Fl (S1041C)	eIF3	124 ± 10	0.230 ± 0.011	0.318 ± 0.016	0.088 ± 0.006
		eIF3-PR*[,f]	75 ± 2	0.194 ± 0.002	0.241 ± 0.004	0.047 ± 0.003

[a] Equilibrium dissociation constants determined by titrating the 42mer-3′Fl or eIF4G-Fl with the binding partners under the experimental conditions.
[b] Anisotropy of the 42mer-3′Fl or eIF4G-Fl prior to addition of any binding partner under the experimental conditions.
[c] Anisotropy of the 42mer-3′Fl or eIF4G-Fl l in the bound state.
[d] Difference between r_{free} and r_{bound}, representing the maximum anisotropy change.
[e] A subsaturating concentration, 200 nM, of eIF3 was used to estimate K_d changes in the presence of eIF3.
[f] eIF3 was cleaved by HIV-1 PR followed by size exclusion chromatography to remove the unbound C terminus of subunit eIF3d.

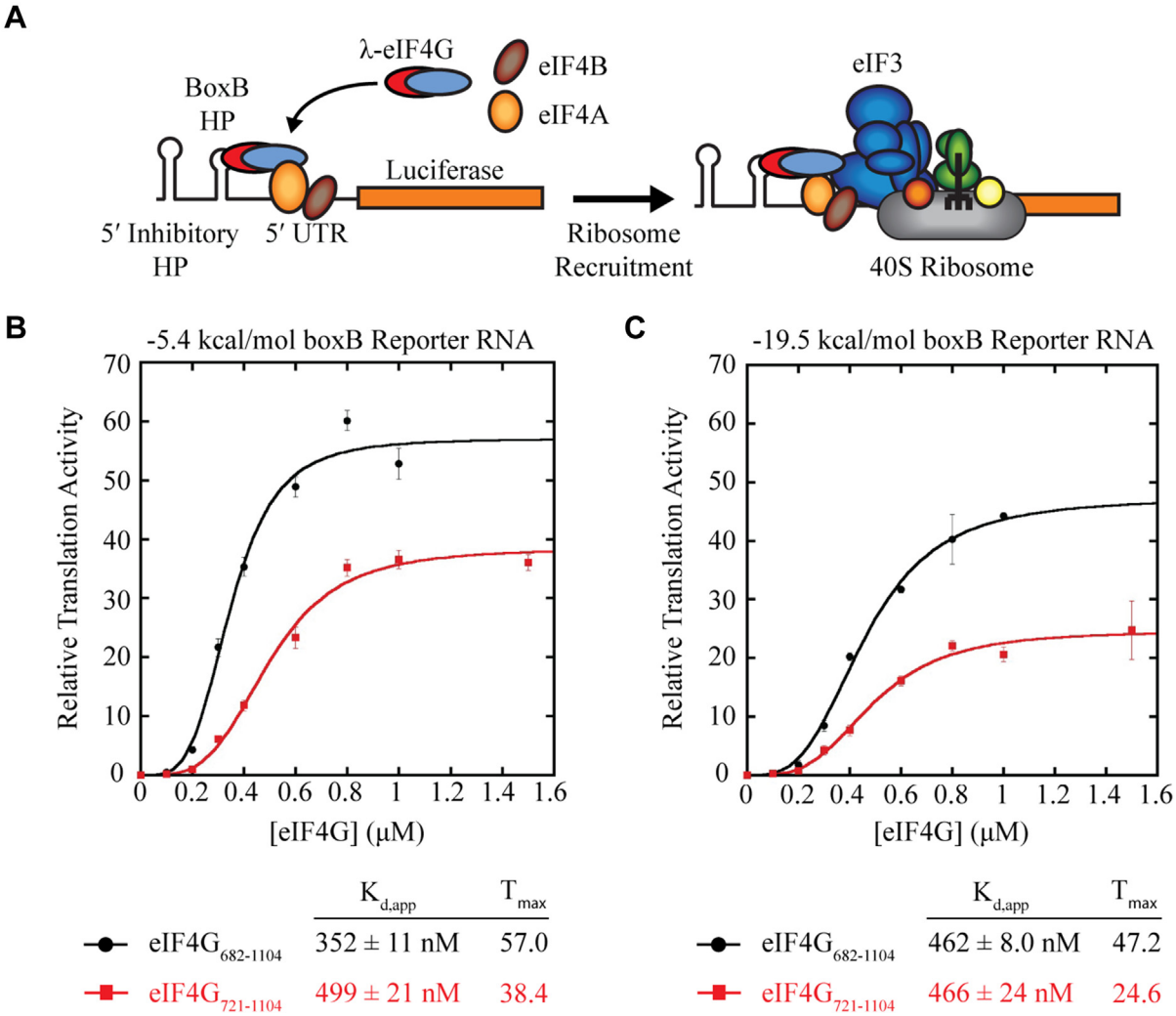

Figure 2. The eIF4G-RBD stimulates translation activity independent of mRNA tethering. *A*, an eIF4G-dependent translation assay mediates reporter RNA recruitment to the ribosome independent of m^7G cap binding. λN-tagged eIF4G constructs are recruited to a renilla luciferase reporter RNA *via* the boxB hairpin (BoxB HP) upstream of the 5′ UTR. An inhibitory stem-loop near the 5′ end of the uncapped RNA prohibits 5′ end-dependent translation, and RNA recruitment to the ribosome occurs solely through interaction with λ-eIF4G. *B* and *C*, relative luciferase translation activity of two different RNA reporters with either *low* (*B*) or *high* (*C*) amounts of secondary structure in the 5′ UTR. λ-eIF4G$_{682\text{-}1104}$ (*black line*) or λ-eIF4G$_{721\text{-}1104}$ (*red line*) was titrated into nuclease-treated RRL and incubated for 20 min at 30 °C prior to measuring renilla luciferase activity, as described in *Experimental Procedures*. The $K_{d,app}$ and maximum relative translation activity ("T_{max}") are the average of three trials and error bars indicate the SEM.

of each complex. Translation activity is normalized to a reaction containing the boxB RNA template in the absence of λ-eIF4G, and this background is subtracted prior to plotting relative translation as a function of λ-eIF4G concentration (see detailed protocol in *Experimental Procedures* and data in Table 2). We tested our system using a reporter RNA with a relatively unstructured 5′ UTR (the region after the boxB hairpin), with a ΔG of −5.4 kcal/mol (Fig. 2*B* and Table 2). Titration of λ-eIF4G$_{682\text{-}1104}$ into the RRL increased the maximum relative translation activity by 57-fold over the background (Fig. 2*B*). In contrast, titration of λ-eIF4G$_{721\text{-}1104}$ increased the maximum relative translation activity by only 38.4-fold translation over the background (Fig. 2*B*). Thus, the presence of the eIF4G-RBD enhances translation by ∼48% compared to the eIF4G construct that does not possess the eIF4G-RBD in this assay. Fitting the increase in translation versus concentration of eIF4G added to a Hill equation (*Experimental Procedures*) reveals a $K_{d,app}$ of 352 ± 11 nM for λ-eIF4G$_{682\text{-}1104}$ and a slightly greater $K_{d,app}$ of 499 ± 21 nM for λ-eIF4G$_{721\text{-}1104}$. While there is a modest reduction in the apparent affinity of translation complexes with the loss of the eIF4G-RBD, there is a clear reduction in maximum translation.

We next tested if an RNA reporter containing a more structured 5′ UTR, with a ΔG of −19.5 kcal/mol, might have a different requirement for an eIF4G containing the eIF4G-RBD than the reporter with a 5′ UTR of −5.4 kcal/mol. Titration of λ-eIF4G$_{682\text{-}1104}$ into the RRL increased the maximum relative translation activity by 47.2-fold over the background (Fig. 2*C* and Table 2). In contrast, titration of λ-eIF4G$_{721\text{-}1104}$ increased the maximum relative translation activity by only 24.6-fold translation over the background (Fig. 2*C*). Thus, the presence of the eIF4G-RBD enhances translation of this increased ΔG reporter by ∼92% compared to the eIF4G construct that does not possess the eIF4G-RBD in this eIF4G-dependent

Table 2
Summary of eIF4G-dependent translation assay activity

Figures	RNA template	λ-eIF4G Conc (μM)	λ-eIF4G$_{682\text{-}1104}$ Luminescence (CPS)	λ-eIF4G$_{682\text{-}1104}$ Relative translation	λ-eIF4G$_{721\text{-}1104}$ Luminescence (CPS)	λ-eIF4G$_{721\text{-}1104}$ Relative translation
Figure 2*B*	−5.4 kcal/mol boxB Reporter RNA	0	18 ± 2	0	17 ± 1	0
		0.1	26 ± 2	0.5 ± 0.11	20 ± 1	0.23 ± 0.1
		0.2	94 ± 9	4.3 ± 0.54	33 ± 2	1.0 ± 0.14
		0.3	403 ± 14	21.7 ± 1.5	120 ± 14	6.2 ± 0.39
		0.4	649 ± 39	35.3 ± 1.6	214 ± 23	11.9 ± 0.93
		0.6	897 ± 91	48.9 ± 1.7	408 ± 55	23.3 ± 1.8
		0.8	1098 ± 97	60.1 ± 1.7	603 ± 58	35.2 ± 1.4
		1	963 ± 69	52.8 ± 2.6	624 ± 46	36.6 ± 1.5
		1.5	-	-	620 ± 70	36.1 ± 1.3
Figure 2*C*	−19.5 kcal/mol boxB Reporter RNA	0	18 ± 1	0	17 ± 1	0
		0.1	24 ± 2	0.3 ± 0.01	22 ± 0.3	0.3 ± 2
		0.2	50 ± 14	1.8 ± 0.8	30 ± 2	0.8 ± 14
		0.3	172 ± 16	8.4 ± 0.9	91 ± 10	4.3 ± 16
		0.4	387 ± 18	20.2 ± 0.7	149 ± 9	7.7 ± 18
		0.6	600 ± 56	31.7 ± 0.5	296 ± 16	16.1 ± 56
		0.8	687 ± 72	40.3 ± 4.3	399 ± 8	22.1 ± 72
		1	829 ± 65	44.2 ± 0.3	376 ± 34	20.6 ± 65
		1.5	-	-	445 ± 84	24.8 ± 65

Translation activity in luminescence counts per second (CPS) is summarized for each boxB renilla luciferase reporter RNA tested with λ-eIF4G$_{682\text{-}1104}$ or λ-eIF4G$_{721\text{-}1104}$.

assay. We calculated almost identical $K_{d,app}$ of 462 ± 8.0 nM and 466 ± 24 nM for λ-eIF4G$_{682\text{-}1104}$ and λ-eIF4G$_{721\text{-}1104}$, respectively (Fig. 2*C*). These data therefore suggest that the eIF4G-RBD is not essential for mRNA translation in this eIF4G-dependent assay, but the amount of secondary structure located in the 5′ UTR does appear to modestly contribute to the degree of eIF4G-RBD-dependent translation that we observe; with a higher ΔG possessing a greater dependency on the eIF4G-RBD. Importantly, because the recombinant eIF4G proteins used are independently tethered to the mRNA via the λN tag, these experiments reveal a novel role of the eIF4G-RBD beyond simply acting as an mRNA tether.

The eIF4G-RBD modestly increases affinity but not unwinding activity of the eIF4A helicase

Since we observe an effect of changes to the ΔG of the 5′ UTR on eIF4G-RBD-dependent translation, we explored the possible role of the eIF4G-RBD as an activator of eIF4A•eIF4B helicase activity using a fluorescence unwinding assay previously developed in our lab (35, 37, 38). For this assay, a 5′-Cy3 labeled RNA oligo is annealed to a template strand adjacent to a spectrally paired 3′-black hole quencher-labeled RNA. Strand separation by the helicase activity of purified eIF4A•eIF4B•eIF4G results in a dramatic increase in Cy3 fluorescence (Fig. 3*A*).

We used a saturating amount of eIF4A and eIF4B (1 μM as described in *Experimental Procedures*) and titrated in eIF4G$_{682\text{-}1104}$ or eIF4G$_{721\text{-}1104}$ to measure eIF4G-dependent duplex unwinding. The normalized initial rate of unwinding (fraction duplex unwound/min) was determined, as described in *Experimental Procedures*, and this was used to calculate the maximum rate of unwinding (A) and the $K_{d,app}$ of the eIF4A•eIF4B•eIF4G•RNA unwinding complex (Fig. 3*B*). For eIF4G$_{682\text{-}1104}$ we calculated a $K_{d,app}$ of 110 ± 13 nM, while eIF4G$_{721\text{-}1104}$ yielded a ∼2-fold greater $K_{d,app}$ of 221 ± 41 nM (Fig. 3*B*). This modest difference in apparent affinity reveals how these initiation factors cooperate with each other to form a stable unwinding complex in the absence or presence of the eIF4G-RBD (Fig. 1*C*). Interestingly, eIF4G$_{682\text{-}1104}$ and eIF4G$_{721\text{-}1104}$ had near identical maximum initial rates of unwinding, at 0.171 and 0.166 fraction duplex unwound/min, respectively (Fig. 3*B*). Thus, while there is a small deficiency in the apparent affinity of the eIF4A•eIF4B•eIF4G$_{721\text{-}1104}$•RNA complex, this can be overcome with higher concentrations of eIF4G$_{721\text{-}1104}$ to yield a very similar maximum initial unwinding rate as eIF4G$_{682\text{-}1104}$. In contrast, maximum relative translation activity was reduced by ∼33 to 50% in the absence of the eIF4G-RBD (Fig. 2). Thus, these data suggest that the eIF4G-RBD is likely not promoting translation by coordinating the eIF4A helicase, at least not in the absence of the 40S subunit.

eIF4G binds the 40S subunit independently of other initiation factors

We next inferred that if eIF4G is not promoting translation through coordination with the mRNA and helicase complex alone, it may be interacting directly or indirectly with the 40S subunit. To this end, we used a native gel electrophoresis assay to visualize eIF4G binding to the 40S subunit in the absence or presence of eIF3 and eIF4A.

We expressed and purified cysteine-free versions of eIF4G$_{682\text{-}1104}$ and eIF4G$_{711\text{-}1104}$, where all native cysteines have been converted to alanine, and where the residue E711 has been mutated to cysteine for site-specific modification with a Cy5 fluorophore to produce eIF4G-Cy5. The cysteine residues are not conserved in eIF4G, and we have no reason to suspect the mutations affect eIF3 or eIF4A binding (7). We note that for these assays the eIF4G-RBD is not completely truncated. To allow fluorescent labeling at residue E711C for both constructs used in native gel electrophoresis and fluorescence polarization assays, we created eIF4G$_{711\text{-}1104}$ by removing the first 29 amino acids of the eIF4G-RBD, leaving the 10 C-terminal amino acids, including two of the eight positively charged residues (Fig. 1*B*). The eIF4G$_{711\text{-}1104}$ construct may retain some RNA

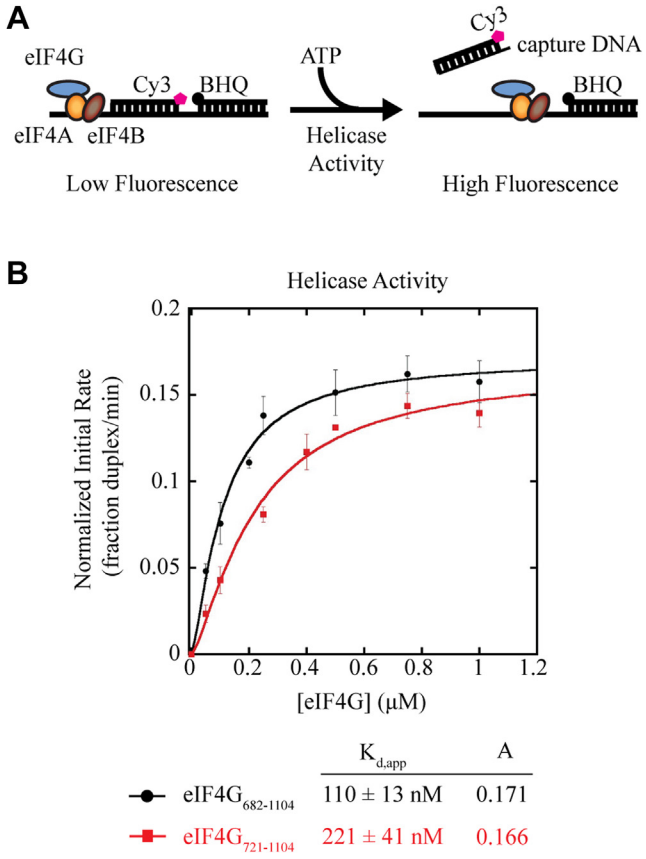

Figure 3. The eIF4G-RBD does not regulate the unwinding activity of the eIF4A helicase. *A*, schematic of eIF4A helicase fluorescent duplex unwinding assay. Briefly, a reporter RNA strand is modified on its 5′ end with Cy3 and annealed adjacent to a spectrally paired black hole quencher (BHQ) on a 3′-end modified RNA to a complimentary loading strand. Reporter RNA is incubated with 1 μM eIF4A, 1 μM eIF4B, and increasing amounts of $eIF4G_{682\text{-}1104}$ or $eIF4G_{721\text{-}1104}$. The addition of ATP/$MgCl_2$ starts the unwinding reaction, resulting in strand separation that is visualized as an increase in Cy3 fluorescence. A DNA capture strand prevents the reannealing of the Cy3 reporter RNA. *B*, The apparent equilibrium dissociation constant ($K_{d,app}$) and maximum initial rates of unwinding ("A") for the eIF4A•eIF4B•eIF4G complex containing $eIF4G_{682\text{-}1104}$ (*black line*) or $eIF4G_{721\text{-}1104}$ (*red line*) are calculated as previously described (see *Experimental Procedures*). Each data point represents the average of at least three experiments and error bars indicate the SEM, where the initial rate of helicase activity (fraction of duplex unwound/min) is calculated from the linear portion of the unwinding curve for the eIF4G concentration indicated.

affinity, but as shown in the assays below it is severely reduced compared to the $eIF4G_{682\text{-}1104}$ construct containing the full-length eIF4G-RBD. We confirmed both eIF4G-Cy5 constructs had similar levels of modification and were not degraded by the procedure using SDS PAGE (Fig. 4*A*). We incubated 100 nM eIF4G-Cy5, 300 nM 40S subunits, 2 μM eIF4A, and 600 nM eIF3 in various combinations in the presence of 0.5 mM ATP-Mg on ice for 10 min followed by 30 °C for 5 min. Complexes were then separated on a 0.8% agarose gel to determine which factors were necessary for complex formation. Each gel was imaged for Cy5 visualization to track eIF4G and then stained with ethidium bromide to observe 40S subunits.

We found that $eIF4G_{682\text{-}1104}$-Cy5 alone or with 2 μM eIF4A (a saturating amount based on previous studies (32, 37)) largely remains in the well and does not enter the gel unless eIF3 is present (Fig. S2). Unexpectedly, $eIF4G_{682\text{-}1104}$-Cy5 enters the gel and comigrates with the 40S subunit in the absence or presence of eIF4A (Fig. 4*B*). Because $eIF4G_{682\text{-}1104}$ and eIF4A are relatively small compared to the 40S subunit, they do not substantially change the migration of the 40S subunit (Fig. 4*B*, lanes 1–3, top and bottom). The addition of eIF3 to form a 40S•eIF4A•eIF3•$eIF4G_{682\text{-}1104}$-Cy5 complex appears to modestly enhance the interaction between $eIF4G_{682\text{-}1104}$-Cy5 and the 40S subunit (Fig. 4*B*, lane 4, top). As expected, the binding of eIF3 causes a sizeable upward shift of the 40S subunit (Fig. 4*B*, lane 4, bottom). The presence of apparent positive cooperativity between $eIF4G_{682\text{-}1104}$-Cy5 and eIF3 in binding to the 40S subunit in this assay may reflect an increase in stability provided by the additional binding site that eIF3 possesses for eIF4G (7, 39). In the absence of the 40S ribosomal subunit, we note that eIF4A•eIF3•$eIF4G_{682\text{-}1104}$-Cy5 forms a stable complex (Fig. 4*B*, lane 5, top panel).

We then compared ribosome and initiation factor complex formation using $eIF4G_{711\text{-}1104}$-Cy5, which lacks the majority of the eIF4G-RBD (10 amino acids remain to allow fluorescent modification). In this assay, we detect very minimal formation of a 40S•$eIF4G_{711\text{-}1104}$-Cy5 or 40S•eIF4A•$eIF4G_{711\text{-}1104}$-Cy5 complex (Fig. 4*B*, lanes 6–7, top). The addition of eIF3 appreciably stabilizes $eIF4G_{711\text{-}1104}$-Cy5 binding to the 40S subunit and resulted in a similar upward shift as seen previously (Fig. 4*B*, lanes 4 and 8). We confirmed $eIF4G_{711\text{-}1104}$-Cy5 can still form a complex with eIF4A and eIF3 (Fig. 4*B*, lane 9), and that $eIF4G_{711\text{-}1104}$ binding to eIF3 is unchanged in the presence of eIF4A (7). Taken together, we interpret the data to indicate that the eIF4G-RBD possesses an independent binding domain for the 40S subunit that is separate from the binding site on eIF4G for the eIF3 complex. As mentioned above, we note that there appears to be some degree of positive cooperativity between eIF4G and eIF3 binding to the 40S subunit, suggesting that the two binding sites may communicate with each other to result in maximum eIF4G binding affinity to the 40S subunit.

To extend these results and test if the second eIF4A binding domain in the C-terminal domain of eIF4G affects 40S subunit binding, we also tested $eIF4G_{682\text{-}1599}$-Cy5 and $eIF4G_{711\text{-}1599}$-Cy5 under the same conditions. We confirmed both eIF4G-Cy5 constructs had similar levels of modification and were not degraded by the procedure using SDS PAGE (Fig. S3*A*). The $eIF4G_{682\text{-}1599}$-Cy5 construct directly binds the 40S ribosome in a similar way to $eIF4G_{682\text{-}1104}$-Cy5 (Fig. S3*B*, lanes 2–5). Interestingly, we observe that the eIF4G-RBD truncation, $eIF4G_{711\text{-}1599}$-Cy5, appears to bind the 40S subunit to a greater degree than $eIF4G_{711\text{-}1104}$-Cy5 (Fig. S3*B*, lane 6, *versus* Fig. 4*B* lane 6). While this binding is appreciably less than observed for $eIF4G_{682\text{-}1599}$-Cy5, this weak binding may suggest an uncharacterized RNA binding region exists in the C-terminal third of eIF4G. Consistent with this, both $eIF4G_{682\text{-}1599}$ and $eIF4G_{711\text{-}1599}$ have a higher binding affinity for RNA in a fluorescence polarization assay than their C-terminal domain truncated counterparts (Fig. S3*C*, Table S2, and Fig. 1*C*). It is also possible that the C-terminal domain cooperates with the eIF4G core to promote its RNA binding

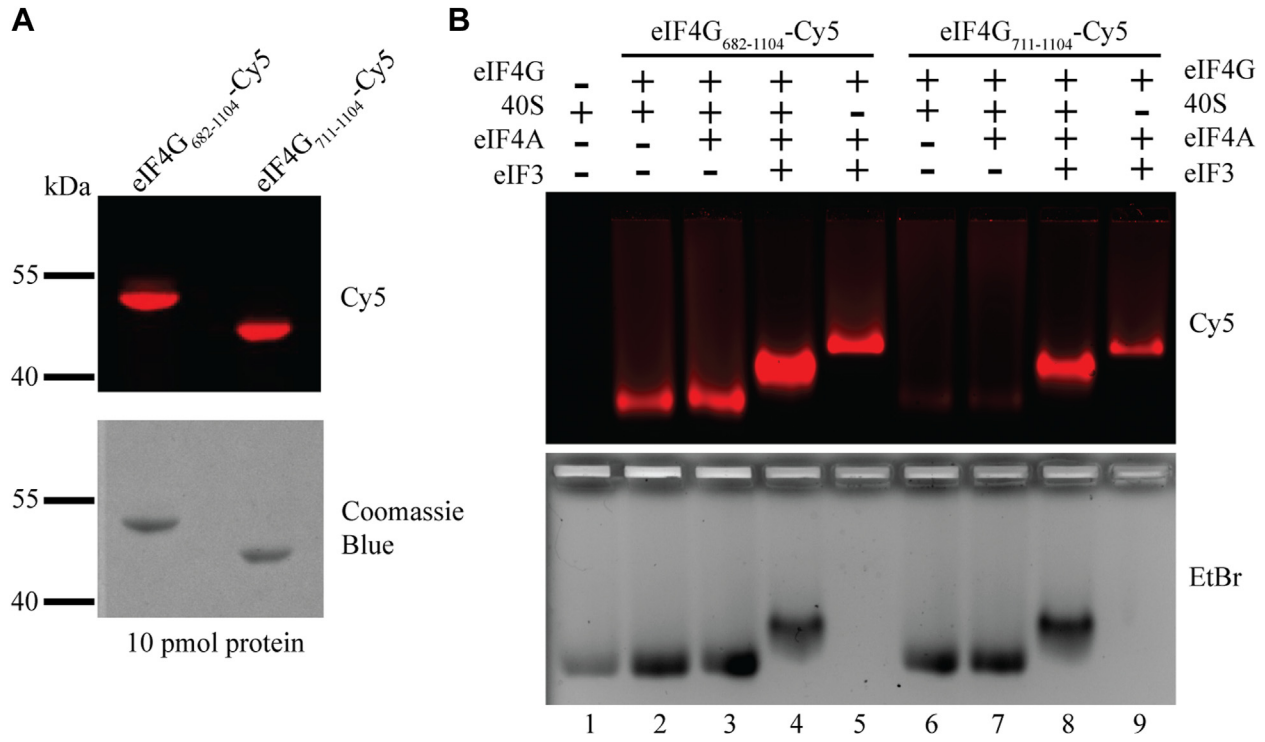

Figure 4. Native gel electrophoresis shows that the eIF4G-RBD stabilizes eIF4G binding to the 40S subunit in the absence of other initiation factors. *A*, cysteine-free eIF4G$_{682\text{-}1104}$ and eIF4G$_{711\text{-}1104}$ constructs each have a single cysteine mutation at residue E711 for site-specific modification with Cy5. Following modification, 10 pmol of each protein was separated by SDS-PAGE, imaged to visualize the Cy5 fluorophore, and stained with Coomassie blue to confirm the purity of each sample and equal levels of Cy5 modification efficiency. *B*, 40S subunits (300 nM), eIF4A (2 μM), eIF3 (600 nM), and eIF4G-Cy5 (100 nM) were incubated together for 10 min on ice followed by 5 min at 30 °C in various combinations and then separated by native gel electrophoresis to visualize complex formation. Gels were imaged to visualize the eIF4G-Cy5 (*upper panel*) and stained with ethidium bromide to directly observe the 40S subunit (*lower panel*). The formation of eIF4G$_{682\text{-}1104}$-dependent complexes (lanes 2–5) and eIF4G$_{711\text{-}1104}$-dependent complexes (lanes 6–9) are shown. The outline of the wells is visible in the lower panel.

affinity. Interestingly we note that upon the addition of eIF4A, the 40S•eIF4G$_{711\text{-}1599}$-Cy5 complex formation appears to be slightly reduced, only to be restored upon the addition of eIF3 (Fig. S3*B*, lanes 7 and 8, top). This is a similar effect to that observed for eIF4A binding to eIF4G$_{711\text{-}1104}$ (Fig. 4*B*, lanes 6–8). This small but reproducible anti-cooperative 40S binding by eIF4G and eIF4A likely reflects an altered conformation of eIF4G when bound to eIF4A. Taken together, these data show that eIF4G can stably and independently bind the 40S subunit through the eIF4G-RBD and that this interaction is a separate binding site from the previously characterized eIF4G•eIF3 interaction.

eIF3 enhances eIF4G recruitment to the 40S subunit independent of the eIF4G-RBD

One disadvantage of the native gel assay is that it is not an equilibrium binding assay. To gain a more rigorous understanding of the interaction between eIF4G and the 40S subunit, we therefore quantitatively analyzed eIF4G binding to the 40S subunit using an equilibrium fluorescence polarization assay. To this end, we labeled the same single cysteine residue, E711C, with fluorescein to create eIF4G$_{682\text{-}1104}$-Fl and eIF4G$_{711\text{-}1104}$-Fl and used these to monitor binding to the 40S subunit. For these experiments, we focused on using an eIF4G•eIF4A•ATP complex since we reasoned that it is the most physiologically relevant complex to characterize. Incubating increasing amounts of the 40S subunit with 20 nM eIF4G$_{682\text{-}1104}$-Fl or eIF4G$_{711\text{-}1104}$-Fl in the presence of a saturating amount of eIF4A and 0.5 mM ATP-Mg results in a K_d of 129 ± 9 nM and 563 ± 72 nM for eIF4A•eIF4G$_{682\text{-}1104}$-Fl and eIF4A•eIF4G$_{711\text{-}1104}$-Fl respectively (Fig. 5, *A* and *B*, dotted lines). Thus, there is a ∼4.5-fold reduction in 40S affinity in the absence of the eIF4G-RBD, which is consistent with the reduced binding of eIF4G in the absence of the eIF4G-RBD on the native gel assay. To explore the possible cooperative binding between the eIF4G-RBD and eIF3, we next added 200 nM eIF3 to each reaction in addition to the saturating amount of eIF4A and measured 40S affinity. This concentration of eIF3 results in ∼50% eIF4G-Fl bound and was chosen to give a reasonable estimate of the K_d of the 40S•eIF4A•eIF3•eIF4G-Fl complex. Upon addition of this sub-saturating amount of eIF3, we measured a K_d of 76 ± 4 nM for eIF4G$_{682\text{-}1104}$-Fl and 248 ± 64 nM for the RNA binding truncation eIF4G$_{711\text{-}1104}$-Fl (Fig. 5, *A* and *B*, solid lines). These data reveal that both eIF4G$_{682\text{-}1104}$-Fl and eIF4G$_{711\text{-}1104}$-Fl bind to the 40S subunit with a modest ∼2-fold increase in affinity in the presence of eIF4A and eIF3. Thus, the binding site provided by eIF3 appears to stabilize the eIF4G•eIF4A•40S complex independently of the eIF4G-RBD.

One limitation of the anisotropy assay is that changes in fluorescence polarization are dependent on a large difference

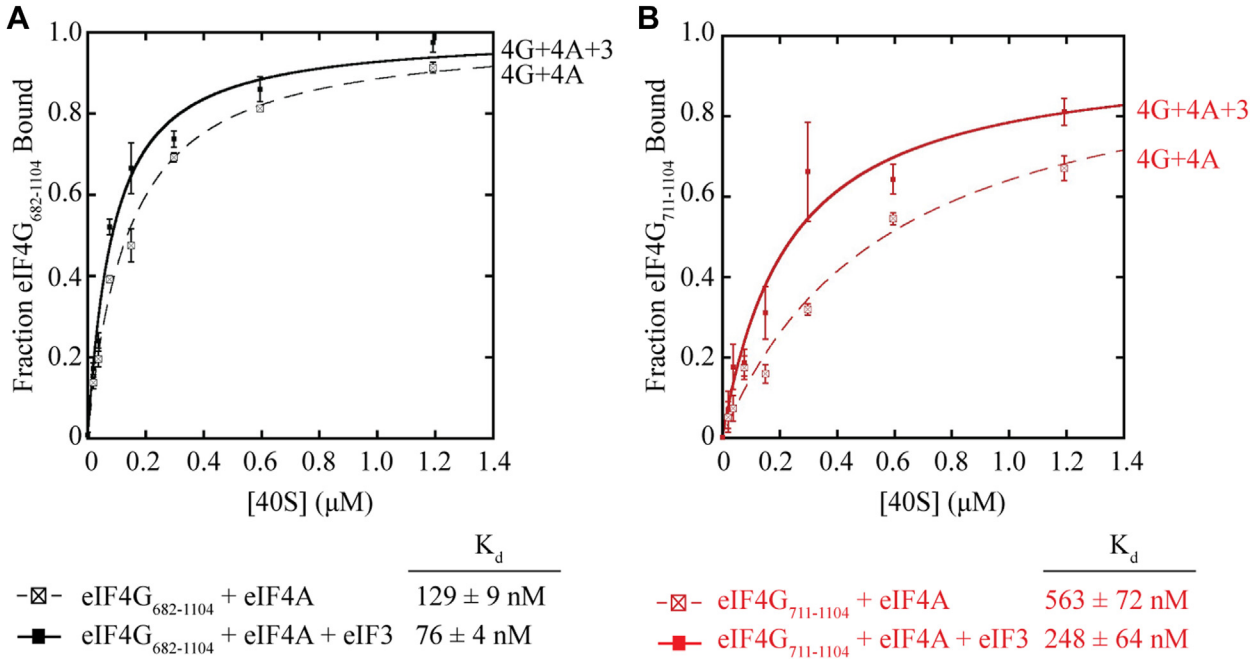

Figure 5. eIF3 enhances eIF4G recruitment to the 40S subunit independently of the eIF4G-RBD. *A*, equilibrium binding of eIF4G$_{682-1104}$-Fl to the 40S subunit together with 3 μM eIF4A in the presence (*solid black line*) or absence (*dashed black line*) of 200 nM eIF3, as measured by the anisotropy assay. *B*, equilibrium binding of eIF4G$_{711-1104}$-Fl to the 40S subunit together with 3 μM eIF4A in the presence (*solid red line*) or absence (*dashed red line*) of 200 nM eIF3. For each experiment, the fraction of eIF4G-Fl bound at different concentrations of 40S subunit is shown. The data are the average of at least three trials and error bars indicate the SEM. Equilibrium binding data were fit to determine the equilibrium dissociation constant (K_d) of eIF4G binding to the 40S subunit, as detailed in the *Experimental Procedures*.

in size of the labeled molecule and binding partner, or a large conformation change upon binding. As more binding partners (especially eIF3) are added to eIF4G-Fl, we note that the total change in fluorescence polarization is appreciably reduced in our assay (Table 1). In addition, the total change in anisotropy for eIF4G$_{711-1104}$-Fl is appreciably smaller than for eIF4G$_{682-1104}$-Fl making it more challenging to use this assay to study the binding of this protein to the 40S subunit (Table 1). Nevertheless, the anisotropy data show that an eIF4G•eIF4A•ATP•eIF3 complex binds directly to the 40S subunit with high affinity, and a clear reduction in 40S binding affinity is observed in the absence of the eIF4G-RBD.

HIV-1 protease cleavage of eIF3d does not affect the eIF4G•eIF3 interaction

When RRL is treated with FMDV L^{pro}, the resulting C-terminal domain of eIF4G (682–1599) remains bound to the 40S subunit upon centrifugation (15). In contrast, treatment of RRL with HIV-2 PR releases the resulting C-terminal domain of eIF4G (721–1599) from the 40S subunit upon centrifugation (15). This effect was attributed to the eIF4G-RBD, but subsequent work discovered that HIV-1 PR directly targets and cleaves eIF3d (30), which is one of three subunits known to interact with eIF4G (7). Following cleavage, the N-terminal eIF3d residues (1–114) remain bound to the eIF3 complex, while the C-terminal amino acids of eIF3d (115–548) dissociate (Fig. 6, *A* and *B* and (30)). The recent human 48S cryo-EM structures confirm the placement of eIF3d on the 40S ribosome near eIF4G but with limited resolution (40, 41). We therefore tested whether eIF3d cleavage by HIV-1 PR may contribute to eIF4G binding to eIF3.

We recombinantly expressed HIV-1 PR in *E. coli* and incubated it with purified eIF3 overnight at 4 °C to ensure complete cleavage of eIF3d (Fig. 6, *A* and *B*). We separated the protease from the eIF3 complex by size exclusion chromatography, which retains high-affinity interactions between all subunits of eIF3 except for eIF3j under the conditions used (42). No signs of the protease were detected by SDS PAGE following purification of the proteolyzed eIF3 complex (eIF3-PR*) (Fig. 6*A*, lane 2). As expected, the N-terminal fragment of eIF3d remained bound to the eIF3 complex (Fig. 6, *A* and *B*, eIF3-PR and eIF3-PR* lanes) (30).

We first tested whether eIF3d cleavage affects binding to FLAG-tagged eIF4G$_{1011-1104}$, which contains the minimal region required for eIF3 binding (9, 18), by coimmunoprecipitation with eIF3 or eIF3-PR*. Our results indicate that eIF3 and eIF3-PR* both bind eIF4G to a similar extent (Fig. 6*C*, lanes 3 and 4). To quantitatively measure the affinity of the eIF4G•eIF3 and eIF4G•eIF3-PR*, we used a fluorescence polarization assay using fluorescein-labeled eIF4G$_{721-1104}$, which we have previously characterized (Fig. 6*D* and Table 1) (7). Our data shows that the K_d of the eIF4G$_{721-1104}$•eIF3 intact complex, 81 ± 23 nM is very similar to the eIF4G$_{721-1104}$•eIF3-PR* K_d of 127 ± 15 nM. Thus, eIF3d cleavage does not appear to appreciably affect eIF4G•eIF3 binding.

We used a crosslinking assay to determine if eIF4G directly binds to the N-terminal domain of eIF3d since eIF4G binds the eIF3 and eIF3-PR* complexes with similar affinity. To this end, we cotranslationally incorporated p-Benzoylphenylalanine

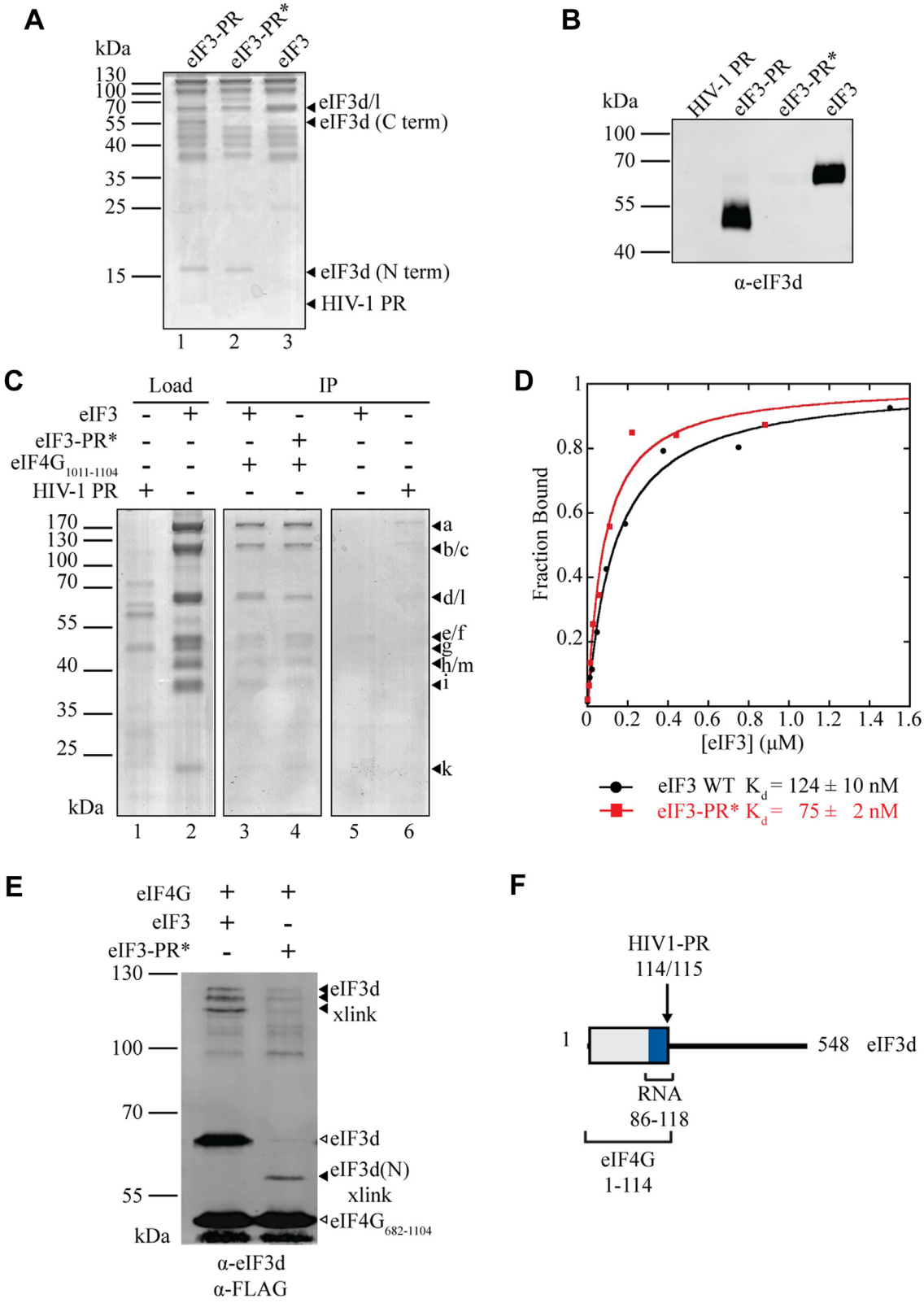

Figure 6. The N-terminal 114 amino acids of eIF3d bind eIF4G. *A*, Coomassie-stained SDS-PAGE gel of eIF3d cleavage by HIV-1 Protease (HIV-1 PR). Asterisk (*) indicates that the sample was purified by gel filtration (as described in *Experimental Procedures*) following proteolysis, which results in dissociation of the eIF3d C-terminal domain from the eIF3 complex. *B*, Western blot confirming eIF3d cleavage and removal of amino acids 115 to 548 from the eIF3 complex following size exclusion chromatography purification. *C*, coimmunoprecipitation assays with Flag-eIF4G$_{1011-1104}$ (the minimal eIF3 binding domain) and eIF3 or eIF3-PR*. *D*, fluorescence polarization assays with eIF4G$_{721-1104}$-Fl and eIF3 or eIF3-PR* to measure eIF4G affinity before and after HIV-1 PR cleavage of the eIF3 complex. *E*, crosslinking with Bpa-labeled Flag-eIF4G$_{682-1104}$ to intact eIF3 or eIF3-PR* shows eIF4G binds to the N-terminus of eIF3d following HIV-1 PR cleavage. *F*, model summarizing eIF3d subunit binding domains and cleavage sites.

(Bpa) into Flag-tagged eIF4G$_{682\text{-}1104}$ at an amber stop codon (S1041X) to create Flag-eIF4G$_{682\text{-}1104}$-Bpa, which is the same method we previously used to crosslink eIF4G$_{1011\text{-}1104}$ to eIF3 (7). Upon incubation with eIF3 and activation by UV light, Flag-eIF4G$_{682\text{-}1104}$-Bpa forms covalent bonds with eIF3 subunits in the eIF4G binding pocket, resulting in a shift in the apparent molecular weight of FLAG-eIF4G$_{682\text{-}1104}$-Bpa by the size of the covalently-bound eIF3 subunit. To identify bound eIF3 subunits we separated crosslinked products by SDS PAGE and analyzed by immunoblot. The eIF4G$_{682\text{-}1104}$-Bpa crosslinks to eIF3d in both eIF3 and eIF3-PR* complexes (Fig. 6*E*). When Flag-eIF4G$_{682\text{-}1104}$-Bpa is incubated with the intact eIF3 complex, the ∼50 kDa Flag-eIF4G$_{682\text{-}1104}$-Bpa band is shifted by ∼65 kDa, the apparent size of the intact eIF3d subunit. The crosslinked species separate into three bands just below the 130 kDa marker (Fig. 6*E*, lane 1). The appearance of multiple bands is possibly due to different crosslinking sites on eIF3d, similar to our previous observation using eIF4G$_{1011\text{-}1104}$-Bpa (7). When Flag-eIF4G$_{682\text{-}1104}$-Bpa is incubated with eIF3-PR* the crosslinked species shifts by only ∼15 kDa, consistent with the size of the eIF3d N-terminal fragment that remains bound to the eIF3 complex following HIV-1 PR cleavage and purification (Fig. 6*E*, lane 2). Together, these results indicate that cleavage of eIF3d does not affect the affinity of eIF3•eIF4G binding, consistent with the eIF4G binding domain residing in the N-terminal 114 amino acids of eIF3d.

Discussion

In this work, we have characterized the human eIF4G-RBD, a lysine/arginine/proline-rich region shown previously to have general RNA binding capabilities and assumed to contribute to the eIF4F binding and recruitment of mRNA (14, 16, 22, 31). To understand the function of RNA binding by the eIF4G-RBD, we used an eIF4G-dependent translation assay to compare the translation efficiency of eIF4G constructs in the presence or absence of the eIF4G-RBD (Fig. 2). Our work shows that the eIF4G-RBD stimulates translation by up to 2-fold when eIF4G is directly tethered to an RNA transcript. Tethering eIF4G to the mRNA circumvents the need for the cap-binding protein eIF4E and enables one to separate a possible role of eIF4G-dependent "tethering" of the mRNA from other potential RNA binding functions. As such, the function of the eIF4G-RBD appears to go beyond simple tethering of the mRNA to the eIF4F complex since the high-affinity boxB•λN-tag interaction cannot compensate for the presence of the eIF4G-RBD in translation assays. Previous work showed that switching the eIF4G-RBD with the RRM of the La autoantigen (in the absence of the eIF4A and eIF3 binding domains) substituted for the eIF4G-RBD in promoting chemical crosslinking of eIF4E with the m^{7}G cap (22). While that experiment indicates that non-specific RNA binding is important for promoting eIF4E binding to the m^{7}G cap, we note that those experiments were carried out using an eIF4G construct that did not include the middle domain or C-terminal domain. It is therefore unknown if switching the eIF4G-RBD for the RRM of the La autoantigen could promote translation in a similar way to the eIF4G-RBD.

Increasing the predicted ΔG of the 5′ UTR of the boxB reporter assay has a noticeably larger inhibitory effect on eIF4G-dependent translation in the absence of the eIF4G-RBD compared to its presence (Fig. 2). This raised the possibility that the eIF4G-RBD may function to coordinate the helicase activity of eIF4A. Using a kinetic duplex unwinding assay shows that the eIF4G-RBD does contribute slightly to the apparent affinity of the eIF4A•eIF4B•eIF4G unwinding complex, but it does not substantially increase helicase activity since both constructs possess a similar maximum initial rate of unwinding upon saturation (Fig. 3). These results, therefore, indicate an alternative role beyond mRNA tethering and eIF4A helicase activity for the eIF4G-RBD during translation initiation in mammals.

Next, we turned our attention from eIF4G binding mRNA to test for a potential interaction with the 40S subunit. Using native gel electrophoresis and fluorescence polarization revealed a novel direct interaction between eIF4G and the 40S subunit. Truncating the eIF4G-RBD appreciably reduced eIF4G•4A•ATP binding to the 40S subunit by over 4-fold, indicating that the eIF4G•40S interaction is strongly enhanced by the eIF4G-RBD even in the presence of eIF4A and ATP (Figs. 4*B* and 5 and S3). Interestingly, we recently showed that non-specific RNA binding by the eIF4F complex is regulated by the nucleotide-bound state of eIF4A (32). Here, we have only tested the contribution that eIF4A makes on eIF4G binding to the 40S subunit in the presence of ATP (Figs. 4 and 5). It will be interesting in the future to rigorously determine if the nucleotide-bound state of eIF4A regulates eIF4G binding to the 40S subunit using a kinetic assay similar to that used for studying the non-specific binding of eIF4F to RNA. We note that the eIF4G-Fl anisotropy signal that we currently possess is rather low, so this would need to be optimized to enable such a rigorous kinetic analysis to be made.

The binding of eIF4G to the 40S subunit is enhanced by eIF3 in the presence or absence of the eIF4G-RBD (Figs. 4*B* and 5, and S3). This finding shows that eIF4G recruitment via eIF3 or the eIF4G-RBD are independent. While we note a modest degree of positive cooperativity is observed between these binding domains in the native gel assay, no such cooperativity was observed in the equilibrium binding assay. As mentioned above, a kinetic analysis of eIF4G binding to the 40S subunit and the relative contributions that the eIF4G-RBD and eIF3 binding domains have on this interaction will be the focus of a future study. We also note that in the absence of the eIF4G-RBD, eIF4G$_{711\text{-}1104}$-Fl binds directly to the 40S subunit in the fluorescence polarization assay as opposed to the gel shift assay (Figs. 4 and 5). This may reflect the 10 amino acids (including two positively charged residues) of the eIF4G-RBD that remain in the constructs used for these assays to allow for fluorescent labeling. Additionally, because the fluorescence polarization assay is at equilibrium, this could maintain interactions that would otherwise dissociate during the native gel assay. Alternatively, this could reflect an additional interaction between the HEAT repeat domain of eIF4G and the 40S subunit that has not yet been observed in the high-resolution cryo-EM structure of the 48S complex (40).

Revealing a direct interaction between the eIF4G-RBD and 40S subunit is consistent with previous work from the Ohlmann lab showing that eIF4G in RRL co-sediments with a ribosome pellet in sucrose gradients when untreated or pre-incubated with L^{pro}, but not HIV-2 PR despite eIF3•40S co-sedimentation remaining unchanged (Fig. 1*A* and (15)). This work revealed many interesting observations, but it was not able to reveal a direct interaction between eIF4G and the 40S subunit since the work was done in RRL where many other factors are present. Subsequent work showed that both eIF4G and its binding partner eIF3d can be targeted by HIV-1 PR, which in turn could have explained the loss of eIF4G•eIF3•40S co-sedimentation in RRL (7, 30). Our recent cryo-EM reconstructions of the 48S complex indicate that the N-terminal domain of eIF3d is located close to the eIF4F complex (40). We directly tested if eIF3d cleavage can reduce the eIF4G•eIF3 interaction using fluorescence polarization and crosslinking assays. Consistent with the 48S structural models, we show that eIF4G binds to the N-terminal 114 amino acids of eIF3d that remain bound to the eIF3 complex upon cleavage by HIV-1 PR, and no affinity change is observed between the cleaved and uncleaved eIF3 complex and eIF4G (Fig. 6 and Table 1). Overall, these data support the conclusion that loss of the eIF4G-RBD results in loss of 40S subunit binding independent of the eIF4G•eIF3 interaction.

Our data shows that the eIF4G-RBD plays an important role in promoting efficient translation through direct binding with the 40S subunit. Thus, eIF4G can interact with the 40S subunit directly via its eIF4G-RBD and indirectly through the eIF3 binding domain (Fig. 7). This prompts the question of where on the 40S subunit the eIF4G-RBD binds. Our recent cryo-EM structure of the 48S complex during scanning places eIF4G near the mRNA exit channel, revealing that mRNA is likely recruited to the 40S ribosome through a "slotting" mechanism. Unfortunately, there is no indication of the location of the eIF4G-RBD in this structure. It is also not clear whether the eIF4G-RBD plays a role at a different stage of initiation, such as an early step in mRNA recruitment. The 48S complex structure does, however, place constraints on possible binding sites, and future biochemical and structural studies may be able to precisely locate eIF4G-RBD-interacting residues or nucleotides on the 40S subunit (40).

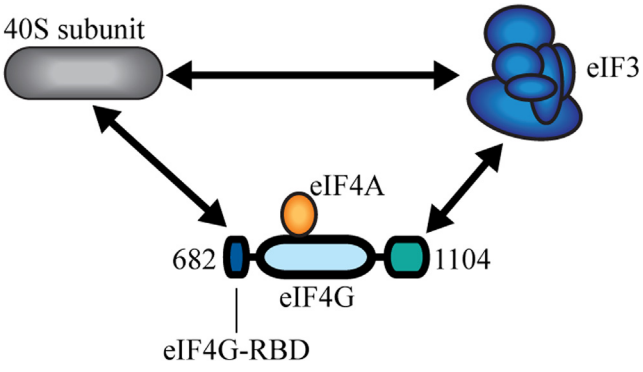

Figure 7. eIF4G binds to the 40S subunit through multiple contacts. Human eIF4G uses multiple interactions to form a molecular bridge that connects the eIF4F cap-binding complex and the 40S subunit. An eIF3-specific binding domain (colored *green*) in human eIF4G indirectly stabilizes eIF4G on the 40S subunit. In this study, we characterize an unexpected direct interaction between the eIF4G-RBD (*colored dark blue*) and the 40S subunit that increases translation independently of mRNA tethering.

We previously characterized the presence of an autoinhibitory domain in human eIF4G that is relieved by the addition of eIF4E to promote eIF4A-dependent helicase activity (35, 43). Interestingly, recent work has shown that the RNA2 domain in yeast eIF4G, which is positioned in a region analogous to the eIF4G-RBD, promotes the closed state of eIF4A, thereby increasing the RNA affinity and helicase activity of eIF4A (44). While we do not observe any clear role of the eIF4G-RBD in promoting eIF4A helicase activity in our assays, it will be important for future work to determine if the 40S subunit binding function of the human eIF4G-RBD is conserved in RNA2 of yeast eIF4G. If RNA2 has a conserved 40S subunit binding function, it may help explain why an eIF3 binding domain in yeast eIF4G has not been observed. It is possible that humans may have evolved an independent eIF3•eIF4G interaction in addition to the eIF4G-RBD•40S interaction, while only a direct yeast eIF4G-RNA2•40S ribosome interaction may be sufficient for mRNA recruitment to yeast ribosomes.

The eIF4G scaffold is a multifunctional translation initiation factor. The role of the eIF4G-RBD in 40S subunit binding characterized in this work is in addition to the roles of eIF4G in eIF4F recruitment to mRNA and in duplex unwinding that is independent of the 48S complex. Detailed biochemical studies into mRNA recruitment and accommodation into the 40S subunit binding channel have revealed unexpected roles for eIF4G, eIF4A, and eIF4E in this process (45). Similar future studies may help determine whether the eIF4G-RBD plays a role in mRNA recruitment. Single-molecule studies comparing 48S complex formation and scanning with wild type or eIF4G-RBD mutant eIF4G proteins may also shed light on which steps of translation initiation are promoted by the eIF4G-RBD, as have been accomplished recently with the yeast translation initiation system (46). While our work has uncovered the importance of the eIF4G-RBD for translation, precisely how this novel interaction regulates mRNA recruitment, accommodation, or scanning, and whether it is targeted for translation regulation *in vivo* remains a topic for future work.

Experimental procedures

Recombinant expression of eIF4G constructs

Recombinant constructs used in this work are denoted by the name of the factor, followed by the amino acid numbers it contains if it is a truncation of the wild-type (WT) factor. All eIF4G constructs are for the human eIF4G1 protein. The numbering of eIF4G constructs is based on UniProt entry Q04637. Our recombinant eIF4G contains a glutamine insertion between residues 696 and 697, as shown in isoforms 7 and 8 (Q04637-7 and Q04637-8), but numbering will be consistent with isoform A as this is currently referred to as the "canonical" sequence in other works.

All eIF4G constructs used in this work were expressed and purified from BL-21(DE3) cells, as previously described, including $eIF4G_{721\text{-}1104}$ (incorrectly listed as $eIF4G_{711\text{-}1104}$ in (7)). Purification λ-eIF4G and Bpa-labeled proteins were according to our previous study (7). Purification of eIF3, eIF4A, and eIF4B has been previously described (7, 37).

Fluorescence polarization assay

eIF4G•RNA affinity was measured using an uncapped 3′ fluorescent-labeled 42-nucleotide (42 nt) RNA as described previously (42-mer RNA-Fl) (32). Briefly, 20 nM 42-mer RNA-Fl was incubated with increasing amounts of $eIF4G_{682\text{-}1104}$, $eIF4G_{721\text{-}1104}$, $eIF4G_{682\text{-}1599}$, or $eIF4G_{721\text{-}1599}$ (as indicated in figures) in Binding Buffer (20 mM Tris acetate (pH 7.5), 70 mM KCl, 2 mM free Mg2+ (supplemented as magnesium acetate), 0.1 mM spermidine, 1 mM DTT, 10% glycerol, and 0.1 mg/ml bovine serum albumin). Each binding reaction was allowed to reach equilibrium at 30 °C for 5 min prior to fluorescence polarization measurements in a Victor X5 Multilabel Plate Reader (PerkinElmer). Each K_d measurement was calculated according to our previous work (47). Each K_d measurement is reported as the average of at least three experiments with error bars indicating the SEM.

eIF4G•40S ribosome affinity was measured using $eIF4G_{682\text{-}1104}$, $eIF4G_{711\text{-}1104}$, $eIF4G_{682\text{-}1599}$, or $eIF4G_{711\text{-}1599}$, which had been expressed and purified with a single cysteine mutation at residue E711C and modified with fluorescein-5-maleimide (eIF4G-Fl). For each reaction, 20 nM eIF4G-Fl was incubated with an increasing amount of 40S subunit ± 3 μM eIF4A ± 200 nM eIF3 (as indicated in each figure) in Binding Buffer supplemented with 0.5 mM ATP/$MgCl_2$. Each reaction was incubated on ice for 10 min, then 30 °C for 5 min, and lastly 10 min at room temperature prior to fluorescence polarization measurements. Each K_d measurement is reported as the average of at least three experiments ± standard error of the mean, and plots show the average of at least three experiments.

BoxB tethered and capped translation assays

The transcription template for the BoxB tethered assay is a derivative of our previously described template and was purchased from GenScript (35). The 5′ UTR was replaced with one of two 5′ UTR sequences possessing different degrees of secondary structure.

−5.4 Reporter RNA 5′ UTR (ΔG = −5.4 kcal/mol) 5′-CTCGAGACACCTACATTTGCTTCGAATATAACTGTGT CACTAGCAACCTCAAACAGAAGCTT-3′

−19.5 Reporter RNA 5′ UTR (ΔG = −19.5 kcal/mol) 5′-CTCGAGACACCTACATTTGCTAGTGATATAACTGTGT CACTAGCAACCTCAAACAGAAGCTT-3′

The predicted stability of each 5′ UTR is determined by using the Predict a Secondary Structure Web Server by the D. H. Mathews lab at the University of Rochester Medical Center (48). BoxB and globin UTR templates are amplified by PCR, *in vitro* transcribed, and purified using phenol-chloroform extraction following standard protocols. Globin UTR reporters remained uncapped or were capped using Faustovirus Capping Enzyme (FCE; NEB) in a 30 μl reaction containing 2 μM RNA, 1X FCE Capping Buffer, 25 U FCE, 0.1 mM SAM, and 0.5 mM GTP. Capping reactions were incubated at 40 °C for 60 min. For data in Figure S1, fresh templates were transcribed and nucleotide contamination was removed from transcription and capping reactions using a Micro Bio-Spin P-6 Gel Column in Tris Buffer (Bio-Rad) prior to phenol extraction. BoxB reporter RNAs are diluted to 25 μM stocks in Folding buffer (20 mM Tris-acetate pH 7.5, 2 mM magnesium acetate, 100 mM KCl, 0.2 mM DTT) and folded by heating to 80 °C, slow cooling to room temperature for ∼1.5 h, then incubating for 10 min on ice (7). Globin RNA reporters were diluted similarly in a folding buffer but without slow cooling.

BoxB translation assays are carried out according to our previous study with minor modifications (7). Briefly, 15 μl reactions contained 60% nuclease-treated rabbit reticulocyte lysate (Promega), 20 μM amino acid mixture minus leucine, 20 μM amino acid mixture minus methionine, 0.5 U/μl Recombinant RNasin Ribonuclease Inhibitor (Promega), 45 mM sodium chloride, 120 mM potassium acetate, 2 mM magnesium acetate, 25 nM uncapped boxB RNA template, and λ-eIF4G at the concentrations specified in figures. These buffer conditions minimize translation in the absence of λ-eIF4G (Fig. S1). For "Kozak" translation buffer conditions in Fig. S1, reactions were carried out in the same way except potassium acetate and magnesium acetate concentrations were 90 mM and 2.2 mM, respectively (36). Reactions are incubated at 30 °C for 20 min prior to luminescence measurement for 10 s on the Victor X5 Multilabel Plate Reader (PerkinElmer) by addition of 75 μl Renilla luciferase substrate (Promega). We normalized luciferase activity to a reaction containing no λ-eIF4G, and then subtracted this background before plotting the relative translation activity as a function of λ-eIF4G concentration (See Table 2 for raw data and normalized translation activity plotted in Fig. 2). Plots in Fig. 2 are fit to the Hill equation:

$$\text{Relative Translation Activity} = T_{max}(x^n)\times\left[{}^{1}/_{(x^n)+(d^n)}\right]$$

Where T_{max} is the maximum relative translation activity; d is the apparent K_d, and n is the Hill coefficient. The average of three reactions ± standard error of the mean is presented here. All data are plotted using KaleidaGraph software (Synergy Software).

Duplex unwinding assay

Unwinding reactions are carried out as previously described (35), using the same template. Briefly, a 24 nt cyanine 3 (Cy3)-labeled RNA reporter strand is annealed 1 nt upstream of a 19 nt black hole quencher (BHQ)-labeled RNA on an uncapped 64 nt RNA loading strand (Fig. 3*A*). These 3 RNAs are annealed at 500 nM in Unwinding Buffer (20 mM Tris-acetate pH 7.5, 2 mM magnesium acetate, 100 mM KCl, 0.2 mM DTT) by heating to 80 °C and slow cooling to room

temperature for ∼1 h. We dilute this annealed stock by half, adding a final 10X molar excess (2.5 μM) of a 24 nt DNA "capture" strand complementary to the Cy-3 reporter RNA, which prevents reannealing following helicase activity. This results in the final 250 nM RNA substrate stock. Unwinding reactions are carried out in 70 μl total volume containing 50 nM annealed RNA substrate (14 μl of the RNA substrate stock), 1 μM each eIF4A and eIF4B, eIF4G in the amount indicated in each figure, and 2 mM ATP/$MgCl_2$ which is added after a stable baseline is reached to start the reaction. All reactions were carried out at room temperature, and data was fit to the Hill equation as described above and in previous works (35, 37).

Native gel electrophoresis

eIF4G•40S ribosome complex formation was visualized using $eIF4G_{682\text{-}1104}$, $eIF4G_{711\text{-}1104}$, $eIF4G_{682\text{-}1599}$, or $eIF4G_{711\text{-}1599}$, which had been expressed and purified with a single cysteine mutation at residue E711C and modified with Cy5 (eIF4G-Cy5). For each reaction, 300 nM 40S subunits, 100 nM eIF4G-Cy5, 2 μM eIF4A and 600 nM eIF3 were combined as indicated in each figure in Binding Buffer supplemented with 0.5 mM ATP/$MgCl_2$. Each reaction was incubated on ice for 10 min, then 30 °C for 5 min prior to loading on a 0.8% agarose gel in THEM Buffer (34 mM Tris acetate (pH 7.5), 57 mM Hepes (pH 7.5), 0.1 mM EDTA, 2 mM magnesium acetate) and separating for ∼5 h at 50 V. Gels were imaged to visualize the Cy5 fluorophore on eIF4G using an Azure Sapphire Biomolecular Imager (Azure Biosystems), then stained with ethidium bromide to directly observe the 40S subunit.

HIV-1 PR Expression and Proteolysis of eIF3

A codon optimized construct of the HIV-1 PR (Strain NL4-3) was purchased from GenScript. The sequence is shown below.

HIV-1 PR (Strain NL4-3)

MPQITLWQRPLVTIKIGGQLKEALLDTGADDTVLEEMN LPGRWKPKMIGGIGGFIKVRQYDQILIEICGHKAIGTVLVG PTPVNIIGRNLLTQIGCTLNF

HIV-1 PR was subcloned into a Pet28c vector with an N-terminal 6X-His-MBP tag with TEV cleavage site, and expressed in 4 L BL-21(DE3) *E. coli* cells for 3 h at 30 °C. HIV-1 PR was purified using a Ni-NTA column using the same buffers and protocol previously described for eIF4G with the following modifications (7). Following elution from the Ni-NTA column HIV-1 PR was dialyzed overnight into Buffer A (20 mM Hepes pH 7.5, 400 mM KCl, 5 mM imidazole, 10% glycerol) with TEV protease to remove the MBP tag. The untagged HIV-1 PR was then passed through the Ni-NTA column to remove MBP and any un-cleaved HIV-1 PR. The flow through containing untagged HIV-1 PR was collected and concentrated using an Amicon Ultra Centrifugal Filter with a 3 kDa molecular weight cutoff (Millipore Sigma). Purified protease was stored at −80 °C.

Proteolysis reactions were carried out overnight at 4 °C with 3 mg/ml eIF3 and 2 mg/ml HIV-1 PR. The cleaved eIF3 complex was separated from HIV-1 PR by gel filtration through a Superose 6 (GE Healthcare) column in a Gel Filtration Buffer (20 mM Hepes pH 7.5, 300 mM KCl, 10% glycerol, 1 mM DTT). The resultant eIF3 complex, eIF3-PR*, retained the N-terminal 114 amino acids of the eIF3d subunit while the C- terminal portion and the eIF3j subunit dissociate at this salt concentration (42). We note that the eIF3c subunit is partially cleaved by HIV-1 PR, but only during gel filtration. This is likely an artifact of the *in vitro* reaction and purification and does not appear to affect eIF4G binding.

eIF4G•eIF3 interaction assays

$eIF4G_{1011\text{-}1104}$ containing N-terminal 6X-HIS and C-terminal FLAG tags was used to coimmunoprecipitate eIF3 or eIF3-PR* using EZview Red Anti-FLAG M2 Affinity Gel (Sigma-Aldrich). Briefly, 10 μg $eIF4G_{1011\text{-}1104}$ in 50 μl binding buffer (BB: 20 mM Hepes pH 7.5, 100 mM KCl, 10% glycerol, 0.5 mM DTT) were pre-incubated with the resin, and the excess was washed twice with 70 μl Wash Buffer (WB: 20 mM hepes pH 7.5, 200 mM KCl, 0.5% TritonX-100, 0.5 mM DTT, 5% glycerol). eIF3 (12 μg) was pre-incubated with HIV-1 PR (or binding buffer for control) to cleave eIF3d, then added to the eIF4G-bound anti-FLAG resin. Once bound, excess eIF3 was washed 3 times with 40 μl WB and eluted in 20 μl of 250 ng/μl FLAG peptide. Results were analyzed by SDS PAGE.

For fluorescence polarization assays, all cysteine residues in $eIF4G_{721\text{-}1104}$ were mutated to alanine by site-directed PCR mutagenesis, and a single cysteine was introduced at S1041 for fluorescein labeling. Amino acids mutated were not conserved and did not appear to affect eIF4A or eIF3 binding functions of this protein. Labeling and fluorescence polarization assays were carried out as described previously. Plots are representative and K_d values shown are the average of at least 3 trials ± standard error of the mean (7).

The cotranslational benzophenone crosslinker incorporation and expression of eIF4G using amber mutants have been previously described in detail. Briefly, the unnatural amino acid p-Benzoylphenylalanine (Bpa; BaChem) is incorporated into $eIF4G_{682\text{-}1104}$ cotranslationally in BL-21 (DE3) *E. coli* at S1041 using the pEVOL plasmid generously provided by Dr Peter Schultz (The Scripps Institute). $eIF4G_{682\text{-}1104}$-Bpa was purified and used in crosslinking reactions with intact eIF3 or eIF3-PR* complexes as described previously (7).

Western blotting

HIV-1 PR cleaved eIF3 and crosslinking reactions were analyzed by immunoblot as described previously (7). Primary antibodies used in this work are mouse monoclonal anti-FLAG nM2 antibody (Sigma-Aldrich) and mouse anti-eIF3d (Santa Cruz Biotech, sc-271515). The secondary antibody used was a Goat anti-Mouse IgG (H + L) secondary antibody fluorescently labeled with DyLight 680. Blots were visualized using the Odyssey Infrared Imaging System (Li-Cor).

Data availability

Data is presented within the manuscript and plasmids and other reagents are available for academic purposes upon request.

Supporting information—This article contains supporting information.

Acknowledgments—We wish to thank the Fraser laboratory for many insightful comments and critical reading of the manuscript.

Author contributions—N. V. and C. S. F. conceptualization; N. V. and C. S. F. methodology; N. V. and C. S. F. project administration; N. V. investigation; N. V. and C. S. F. writing–original draft; N. V. and C. S. F. writing–review and editing.

Funding and additional information—This work was supported by NIH grant R01 GM092927 and R35 GM152137 to CSF. The content is solely the responsibility of the authors and does not necessarily represent the official views of the National Institutes of Health.

Conflict of interest—The authors declare that they have no known competing financial interests or personal relationships that could have appeared to influence the work reported in this paper.

Abbreviations—The abbreviations used are: Bpa, p-Benzoylphenylalanine; cryo-EM, cryo-electron microscopy; eIF3d, eIF3 subunit d; eIF, eukaryotic initiation factor; EMCV, encephalomyocarditis virus; FMDV, foot-and-mouth disease virus; HIV PR, human immunodeficiency virus protease; Lpro, L protease; MBP, maltose binding protein; MNK1, MAPK-activated protein kinase 1; mRNA, messenger RNA; PABP, poly(A) binding protein; RBD, RNA binding domain.

References

1. Fraser, C. S. (2009) The molecular basis of translational control. *Prog. Mol. Biol. Transl. Sci.* **90**, 1–51
2. Hinnebusch, A. G. (2014) The scanning mechanism of eukaryotic translation initiation. *Annu. Rev. Biochem.* **83**, 779–812
3. Fraser, C. S. (2015) Quantitative studies of mRNA recruitment to the eukaryotic ribosome. *Biochimie* **114**, 58–71
4. Shirokikh, N. E., and Preiss, T. (2018) Translation initiation by cap-dependent ribosome recruitment: recent insights and open questions. *Wiley Interdiscip. Rev. RNA* **9**, e1473
5. Sokabe, M., and Fraser, C. S. (2019) Toward a kinetic understanding of eukaryotic translation. *Cold Spring Harbor Perspect. Biol.* **11**, a032706
6. Merrick, W. C. (2015) eIF4F: a retrospective. *J. Biol. Chem.* **290**, 24091–24099
7. Villa, N., Do, A., Hershey, J. W., and Fraser, C. S. (2013) Human eukaryotic initiation factor 4G (eIF4G) protein binds to eIF3c, -d, and -e to promote mRNA recruitment to the ribosome. *J. Biol. Chem.* **288**, 32932–32940
8. Brito Querido, J., Sokabe, M., Diaz-Lopez, I., Gordiyenko, Y., Fraser, C. S., and Ramakrishnan, V. (2022) The structure of a human translational initiation complex reveals two independent roles for the helicase eIF4A. *BioRxiv*. https://doi.org/10.1101/2022.12.07.5.519490
9. Lamphear, B. J., Kirchweger, R., Skern, T., and Rhoads, R. E. (1995) Mapping of functional domains in eukaryotic protein synthesis initiation factor 4G (eIF4G) with picornaviral proteases. Implications for cap-dependent and cap-independent translational initiation. *J. Biol. Chem.* **270**, 21975–21983
10. Prevot, D., Darlix, J. L., and Ohlmann, T. (2003) Conducting the initiation of protein synthesis: the role of eIF4G. *Biol. Cell* **95**, 141–156. S0248490003000315 [pii]
11. Mader, S., Lee, H., Pause, A., and Sonenberg, N. (1995) The translation initiation factor eIF-4E binds to a common motif shared by the translation factor eIF-4 gamma and the translational repressors 4E-binding proteins. *Mol. Cell Biol.* **15**, 4990–4997
12. Tarun, S. Z., Jr., and Sachs, A. B. (1996) Association of the yeast poly(A) tail binding protein with translation initiation factor eIF-4G. *EMBO J.* **15**, 7168–7177
13. Imataka, H., Gradi, A., and Sonenberg, N. (1998) A newly identified N-terminal amino acid sequence of human eIF4G binds poly(A)-binding protein and functions in poly(A)-dependent translation. *EMBO J.* **17**, 7480–7489
14. Goyer, C., Altmann, M., Lee, H. S., Blanc, A., Deshmukh, M., Woolford, J. L., Jr., *et al.* (1993) TIF4631 and TIF4632: two yeast genes encoding the high-molecular-weight subunits of the cap-binding protein complex (eukaryotic initiation factor 4F) contain an RNA recognition motif-like sequence and carry out an essential function. *Mol. Cell Biol.* **13**, 4860–4874
15. Prevot, D., Decimo, D., Herbreteau, C. H., Roux, F., Garin, J., Darlix, J. L., *et al.* (2003) Characterization of a novel RNA-binding region of eIF4GI critical for ribosomal scanning. *EMBO J.* **22**, 1909–1921
16. Lomakin, I. B., Hellen, C. U., and Pestova, T. V. (2000) Physical association of eukaryotic initiation factor 4G (eIF4G) with eIF4A strongly enhances binding of eIF4G to the internal ribosomal entry site of encephalomyocarditis virus and is required for internal initiation of translation. *Mol. Cell Biol.* **20**, 6019–6029
17. Imataka, H., and Sonenberg, N. (1997) Human eukaryotic translation initiation factor 4G (eIF4G) possesses two separate and independent binding sites for eIF4A. *Mol. Cell Biol.* **17**, 6940–6947
18. Korneeva, N. L., Lamphear, B. J., Hennigan, F. L., Merrick, W. C., and Rhoads, R. E. (2001) Characterization of the two eIF4A-binding sites on human eIF4G-1. *J. Biol. Chem.* **276**, 2872–2879
19. De Gregorio, E., Preiss, T., and Hentze, M. W. (1999) Translation driven by an eIF4G core domain *in vivo*. *EMBO J.* **18**, 4865–4874
20. Ali, I. K., McKendrick, L., Morley, S. J., and Jackson, R. J. (2001) Truncated initiation factor eIF4G lacking an eIF4E binding site can support capped mRNA translation. *EMBO J.* **20**, 4233–4242
21. Haghighat, A., and Sonenberg, N. (1997) eIF4G dramatically enhances the binding of eIF4E to the mRNA 5'-cap structure. *J. Biol. Chem.* **272**, 21677–21680
22. Yanagiya, A., Svitkin, Y. V., Shibata, S., Mikami, S., Imataka, H., and Sonenberg, N. (2009) Requirement of RNA binding of mammalian eukaryotic translation initiation factor 4GI (eIF4GI) for efficient interaction of eIF4E with the mRNA cap. *Mol. Cell Biol.* **29**, 1661–1669
23. Park, E. H., Walker, S. E., Lee, J. M., Rothenburg, S., Lorsch, J. R., and Hinnebusch, A. G. (2011) Multiple elements in the eIF4G1 N-terminus promote assembly of eIF4G1*PABP mRNPs in vivo. *EMBO J.* **30**, 302–316
24. Etchison, D., Milburn, S. C., Edery, I., Sonenberg, N., and Hershey, J. W. (1982) Inhibition of HeLa cell protein synthesis following poliovirus infection correlates with the proteolysis of a 220,000-dalton polypeptide associated with eucaryotic initiation factor 3 and a cap binding protein complex. *J. Biol. Chem.* **257**, 14806–14810
25. Devaney, M. A., Vakharia, V. N., Lloyd, R. E., Ehrenfeld, E., and Grubman, M. J. (1988) Leader protein of foot-and-mouth disease virus is required for cleavage of the p220 component of the cap-binding protein complex. *J. Virol.* **62**, 4407–4409
26. Lloyd, R. E., Grubman, M. J., and Ehrenfeld, E. (1988) Relationship of p220 cleavage during picornavirus infection to 2A proteinase sequencing. *J. Virol.* **62**, 4216–4223
27. Perales, C., Carrasco, L., and Ventoso, I. (2003) Cleavage of eIF4G by HIV-1 protease: effects on translation. *FEBS Lett.* **533**, 89–94
28. Ventoso, I., Blanco, R., Perales, C., and Carrasco, L. (2001) HIV-1 protease cleaves eukaryotic initiation factor 4G and inhibits cap-dependent translation. *Proc. Natl. Acad. Sci. U. S. A.* **98**, 12966–12971
29. Alvarez, E., Menendez-Arias, L., and Carrasco, L. (2003) The eukaryotic translation initiation factor 4GI is cleaved by different retroviral proteases. *J. Virol.* **77**, 12392–12400

30. Jager, S., Cimermancic, P., Gulbahce, N., Johnson, J. R., McGovern, K. E., Clarke, S. C., *et al.* (2011) Global landscape of HIV-human protein complexes. *Nature* **481**, 365–370
31. Pestova, T. V., Hellen, C. U., and Shatsky, I. N. (1996) Canonical eukaryotic initiation factors determine initiation of translation by internal ribosomal entry. *Mol. Cell Biol.* **16**, 6859–6869
32. Izidoro, M. S., Sokabe, M., Villa, N., Merrick, W. C., and Fraser, C. S. (2022) Human eukaryotic initiation factor 4E (eIF4E) and the nucleotide-bound state of eIF4A regulate eIF4F binding to RNA. *J. Biol. Chem.* **298**, 102368
33. Van Gilst, M. R., Rees, W. A., Das, A., and von Hippel, P. H. (1997) Complexes of N antitermination protein of phage lambda with specific and nonspecific RNA target sites on the nascent transcript. *Biochemistry* **36**, 1514–1524
34. De Gregorio, E., Baron, J., Preiss, T., and Hentze, M. W. (2001) Tethered-function analysis reveals that eIF4E can recruit ribosomes independent of its binding to the cap structure. *RNA* **7**, 106–113
35. Feoktistova, K., Tuvshintogs, E., Do, A., and Fraser, C. S. (2013) Human eIF4E promotes mRNA restructuring by stimulating eIF4A helicase activity. *Proc. Natl. Acad. Sci. U. S. A.* **110**, 13339–13344
36. Kozak, M. (1990) Evaluation of the fidelity of initiation of translation in reticulocyte lysates from commercial sources. *Nucleic Acids Res.* **18**, 2828
37. Ozes, A. R., Feoktistova, K., Avanzino, B. C., and Fraser, C. S. (2011) Duplex unwinding and ATPase activities of the DEAD-box helicase eIF4A are coupled by eIF4G and eIF4B. *J. Mol. Biol.* **412**, 674–687
38. Özeş, A. R., Feoktistova, K., Avanzino, B. C., Baldwin, E. P., and Fraser, C. S. (2014) Real-time fluorescence assays to monitor duplex unwinding and ATPase activities of helicases. *Nat. Protoc.* **9**, 1645–1661
39. LeFebvre, A. K., Korneeva, N. L., Trutschl, M., Cvek, U., Duzan, R. D., Bradley, C. A., *et al.* (2006) Translation initiation factor eIF4G-1 binds to eIF3 through the eIF3e subunit. *J. Biol. Chem.* **281**, 22917–22932. M605418200 [pii]
40. Brito Querido, J., Sokabe, M., Kraatz, S., Gordiyenko, Y., Skehel, J. M., Fraser, C. S., *et al.* (2020) Structure of a human 48S translational initiation complex. *Science* **369**, 1220–1227
41. Brito Querido, J., Sokabe, M., Diaz-Lopez, I., Gordiyenko, Y., Fraser, C. S., and Ramakrishnan, V. (2024) The structure of a human translation initiation complex reveals two independent roles for the helicase eIF4A. *Nat. Struct. Mol. Biol.* **31**, 455–464
42. Fraser, C. S., Berry, K. E., Hershey, J. W., and Doudna, J. A. (2007) eIF3j is located in the decoding center of the human 40S ribosomal subunit. *Mol. Cell* **26**, 811–819
43. Avanzino, B. C., Fuchs, G., and Fraser, C. S. (2017) Cellular cap-binding protein, eIF4E, promotes picornavirus genome restructuring and translation. *Proc. Natl. Acad. Sci. U. S. A.* **114**, 9611–9616
44. Krause, L., Willing, F., Andreou, A. Z., and Klostermeier, D. (2022) The domains of yeast eIF4G, eIF4E and the cap fine-tune eIF4A activities through an intricate network of stimulatory and inhibitory effects. *Nucleic Acids Res.* **50**, 6497–6510
45. Sokabe, M., and Fraser, C. S. (2017) A helicase-independent activity of eIF4A in promoting mRNA recruitment to the human ribosome. *Proc. Natl. Acad. Sci. U. S. A.* **114**, 6304–6309
46. Wang, J., Shin, B. S., Alvarado, C., Kim, J. R., Bohlen, J., Dever, T. E., *et al.* (2022) Rapid 40S scanning and its regulation by mRNA structure during eukaryotic translation initiation. *Cell* **185**, 4474–4487.e17
47. Sokabe, M., and Fraser, C. S. (2014) Human eukaryotic initiation factor 2 (eIF2)-GTP-Met-tRNAi Ternary complex and eIF3 stabilize the 43S preinitiation complex. *J. Biol. Chem.* **289**, 31827–31836
48. Reuter, J. S., and Mathews, D. H. (2010) RNAstructure: software for RNA secondary structure prediction and analysis. *BMC Bioinformatics* **11**, 129

Nancy Villa is an assistant project scientist in the lab of Dr. Christopher S. Fraser at the University of California, Davis. She is interested in the mechanism and regulation of mRNA recruitment to the ribosome, which she studies using purified components and cell-free extracts in quantitative and kinetic assays. She aims to understand how translation initiation factor availability and posttranslational modifications regulate mRNA translation and how this knowledge may be applied to therapeutics.